Journal of Molecular Structure 1108 (2016) 112–125

Contents lists available at ScienceDirect

Journal of Molecular Structure

journal homepage: http://www.elsevier.com/locate/molstruc

Conformational search, spectral analysis and electronic properties of 5-(4-Pyridinyl)-1,3,4-thiadiazol-2-amine

Vikas K. Shukla [a], Monirah A. Al-Alshaikh [b], Ali A. El-Emam [c], Alok K. Sachan [a], Ruchi Srivastava [a], Onkar Prasad [a], Leena Sinha [a, *]

[a] Department of Physics, University of Lucknow, 226007, Lucknow, India
[b] Department of Chemistry, College of Sciences, King Saud University, Riyadh 11451, Saudi Arabia
[c] Department of Pharmaceutical Chemistry, College of Pharmacy, King Saud University, Riyadh 11451, Saudi Arabia

ARTICLE INFO

Article history:
Received 15 August 2015
Received in revised form
26 November 2015
Accepted 26 November 2015
Available online 2 December 2015

Keywords:
Vibrational analysis
B3LYP
M06-2X
Solute-solvent interaction

ABSTRACT

Comprehensive investigation of molecular geometry and electronic structure of 5-(4-Pyridinyl)-1,3,4-thiadiazol-2-amine in ground as well as in the first excited state has been carried out. The stable conformers of the title compound have been determined from the 3D potential energy scan by varying selected dihedral angles, responsible for conformational flexibility. As the energy difference between the conformers was very small, the relative stability has been confirmed at potentially high-level G2MP2 method. The most stable structure was optimized with B3LYP and M06-2X functional using polarized triple-zeta 6-311++G(d,p), to obtain the ground state structure and calculation of vibrational wavenumbers. Experimental FT-IR and FT-Raman spectra were compared with theoretical spectral data. Dipole moment, polarizability, first static hyperpolarizability and molecular electrostatic potential surface map have been calculated to get a better insight of the properties of title molecule. Frequency-dependent first hyperpolarizability $\beta(-2\omega;\omega,\omega)$ has also been evaluated to gauge the non-linear optical behavior of the title compound. Natural bond orbital (NBO) analysis has been done to study the stability of the compound arising from charge delocalization. UV–Vis spectrum, possible solvent-solute interaction and electronic properties such as frontier orbitals, band gap energies have been calculated by TD-DFT approach. ^{1}H nuclear magnetic resonance chemical shifts of the title compound were calculated using the Gauge-Including Atomic Orbital (GIAO) method and compared with experimental data.

1. Introduction

1,3,4-thiadiazoles, five-membered ring systems containing one sulfur and two nitrogen atoms are one of the most imperative and acclaimed heterocyclic nuclei, being a core structural constituent in a collection of drug classes namely antimicrobial, anti-inflammatory, analgesic, antiviral, antineoplastic, and anti-tubercular agents [1–8]. El-Gohary and Shaaban [9] have synthesized new series of fused 1,3,4 thiadiazoles and reported their antimicrobial, antiquorum-sensing and antitumor activities. Very recently Patel et al. [10]. have synthesized and reported 1,3,4 thiadiazole derivatives as inhibitors of transforming growth factor-β type-I receptor kinase (ALK5). Sulfamethazole, cefazoline, acetazolamide and methazolamide etc. are few drugs containing thiadiazole nucleus. In addition to pharmaceutical zone, the thiadiazoles are also being used in industrial, agricultural and polymer area [11,12]. Synthesis of new thiadiazole derivatives and analysis of their chemical behavior as well as biological activities have achieved prominence in recent decades. Despite extensive spectroscopic studies on thiadiazole and its derivatives [13–19], literature survey reveals that neither Raman, IR and UV–Vis spectroscopic studies nor the quantum chemical calculations on 5-(4-Pyridinyl)-1,3,4-thiadiazol-2-amine (PTA) have been reported so far. To have a decent insight of the structural profile of the compound, a detailed conformational search using 3D potential energy scan at DFT/B3LYP has been obtained by varying selected dihedral angles and relative conformational stability has been confirmed at G2MP2 level. The most stable conformer has been optimized at B3LYP and M06-2X level and vibrational analysis has been performed. Electric moments like Dipole moment, polarizability, first static hyperpolarizability have been calculated at B3LYP and M06-2X

* Corresponding author.
E-mail address: sinhaleena27@gmail.com (L. Sinha).

http://dx.doi.org/10.1016/j.molstruc.2015.11.077
0022-2860/

functionals and compared. Molecular electrostatic potential surface have been drawn at DFT/B3LYP/6311++G(d,p) level of theory. Frequency-dependent first hyperpolarizability $\beta(-2\omega;\omega,\omega)$ has also been evaluated to gauge the non-linear optical behavior of the title compound. Natural bond orbital (NBO) analysis has been applied to study the stability of the molecule arising from charge delocalization. UV–Vis spectrum of the title compound was also recorded and electronic properties, such as frontier orbitals and band gap energies were calculated by TD-DFT approach. The method has also been used to investigate hydrogen bonding interaction between PTA and methanol. Thermo-dynamical properties such as heat capacity, entropy and enthalpy change at various temperatures have been calculated to gain a deeper insight of the thermal characteristics of the title compound. H^1 NMR chemical shifts also have been assigned with the help of calculated and experimental findings.

2. Experimental and computational methods

2.1. Sample and instrumentation

Pure 5-(4-Pyridinyl)-1,3,4-thiadiazol-2-amine (PTA) of spectral grade was purchased from M/s Aldrich Chemical Co., as a white crystalline solid and was used as such without any further purification.

The FT-IR spectrum of the title compound was recorded using Perkin Elmer spectrometer (version 10.03.06) in the region 4000–400 cm^{-1} using KBr pellet method. The FT-Raman spectrum in the region 4000–100 cm^{-1} with a spectral resolution of 0.9 cm^{-1} was recorded on Planer RAME model of Planer RAM micro Raman systems. A 532 nm laser line of single longitudinal mode diode-pumped solid state (SLM-DPSS) laser was used as the exciting wavelength. The UV absorption spectrum of PTA was examined in the range 500–200 nm using the JASCO UV V-670, UV-VIS recording spectrometer. The UV pattern was taken from a 10^{-5} M solution of PTA, dissolved in methanol. All the spectral measurements have been performed at the Indian Institute of Technology, Kanpur.

2.2. Computational details

Density functional theory [20] using B3LYP [21–23] and M06-2X [24] functionals with polarized triple-zeta 6-311++G(d,p) has been used for obtaining the ground state structure and calculation of vibrational wavenumbers. The exceedingly popular B3LYP (Becke, three-parameter, Lee-Yang-Parr) exchange-correlation functional, mixes a certain amount of the exact Hartree–Fock exchange energy into the exchange and correlation obtained from other functionals. The M06 suites of functional are meta-hybrid GGA DFT functional fabricated with empirical fitting of their parameters, but restraining to concept of the uniform electron gas. The suite has a very good response under dispersion forces, and thus fixing one of the biggest deficiencies in DFT methods. The M06-2X, functional is one of the best functional for the study of non-covalent interactions. All calculations in this study have been performed with the Gaussian 09 program package [25] and results are analyzed with the Gaussview 5.0 molecular visualization program [26]. Possible conformers of the title compound have been determined from the potential energy scan at DFT/B3LYP/6-311++G(d,p) level, by varying the N4–C5–C6–C11 and N3–C2–N12–H17 dihedral angles. 3-D Potential energy surface showing the variation of dihedral angles and their corresponding energies are given in Fig. 1(a) and thus obtained stable conformers of the title molecule are shown in Fig. 1(b). Calculated energies of four conformers (Table 1), indicates the conformer B is the most stable one. Due to small energy difference between the conformers, it was essential to confirm the relative stability, which has been done at G2MP2 level. Geometrical structure corresponding to the lowest minima in the potential energy surface (conformer B in Fig. 1)(b) has been used as input for optimizing the structure at B3LYP and M06-2X functionals and for the calculation of vibrational wavenumbers. As X-ray crystallographic data of the compound is not available optimized parameters of the title compound are compared with experimental data of the compound with similar structure [15]. Positive value of all the calculated wavenumbers settles the stability of optimized geometry. An empirical uniform scaling factor of 0.983 up to 1700 cm^{-1} and 0.958 for greater than 1700 cm^{-1} [27,28] was used to offset the systematic errors caused by basis set incompleteness and vibrational anharmonicity [29]. Theoretical vibrational assignment of the title compound using percentage potential energy distribution (PED) has been done with the MOLVIB program (version V7.0-G77) written by T. Sundius [30–32]. The Raman activities (S_i) provided with the Gaussian output were subsequently converted to relative Raman intensities (I_i) using the relationship derived from the basic theory of Raman scattering [33,34]. The calculated Raman and IR spectra were plotted using the pure Lorentzian band shape with a band width of FWHM of 5 cm^{-1}. The theoretical UV–Vis spectrum has been computed by TDDFT method, using 6-311++G(d,p) basis set for gas phase and the solvent effect also has been taken into consideration by implementing IEFPCM model at the same level of theory. IEFPCM is integral equation formalism (IEF) version of the polarizable continuum model (PCM). In this method solute cavity is created via a set of overlapping spheres. The optimized geometry has also been used to calculate dipole moment, mean polarizability and first static hyperpolarizability based on the finite field approach. Frequency-dependent first hyperpolarizability $\beta(-2\omega;\omega,\omega)$ for the second harmonic generation (SHG) were also calculated by couple-perturbed (CP) DFT method with B3LYP functional, at the same basis set, used to calculate static β_{tot}.

Natural bonding orbital (NBO) calculations [35] were performed to understand various second order interactions between the filled orbitals of one subsystem and vacant orbitals of another subsystem which is a measure of the hyper conjugation or intramolecular delocalization. The second order perturbation theory analysis of Fock matrix in NBO basis, was carried out to evaluate the donor-acceptor interactions. For each donor (i) and acceptor (j), the stabilization energy E^2 associated with the delocalization i → j is estimated as

$$E^{(2)} = \Delta E_{ij} = q_i \frac{F(i,j)^2}{\varepsilon_j - \varepsilon_i}$$

Where q_i is the donor orbital occupancy, ε_i and ε_j are diagonal elements and F(i,j) is the off diagonal NBO Fock matrix element. NBO analysis provides a detailed insight into the electronic structure of a system namely-electronic density distribution on atoms, electronic conjugation between the bonds, hybridization as well as binding affinity towards a system.

3. Results and discussion

3.1. Molecular geometry and PES scan studies

Conformational search for the title compound has been performed through potential energy surface (PES) scan at DFT/B3LYP/6-311++G(d,p) level of theory by varying dihedral angles N4–C5–C6–C11 and N3–C2–N12–H17 in steps of 10° from −180° to 180° and all the geometrical parameters were simultaneously relaxed during the scan except the two selected dihedral angles. Dihedral angle N4–C5–C6–C11 and N3–C2–N12–H17 are the

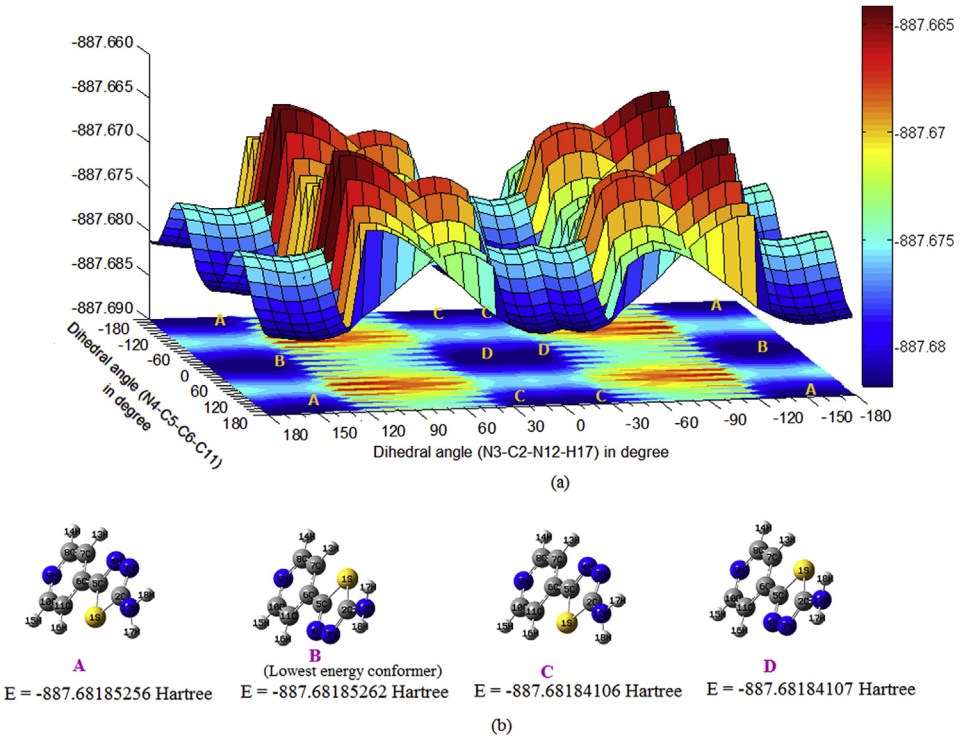

Fig. 1. (a)Potential energy surface scan of 5-(4-Pyridinyl)-1,3,4-thiadiazol-2-amine (PTA). (b)Stable conformers of PTA at DFT/B3LYP/6-311++G(d,p) along with their energies.

Table 1
Energies of various conformers of 5-(4-Pyridinyl)-1,3,4-thiadiazol-2-amine calculated by using B3LYP and G2MP2 methods.

Conformers	B3LYP (Hartree)	G2MP2 (Hartree)
A	−887.68185256	−886.240400
B	−887.68185262	−886.240401
C	−887.68184106	−886.240402
D	−887.68184107	−886.240404

relevant torsional angles, which decide conformational flexibility within the title molecule. The torsional profiles of PES scan are shown in Fig. 1 (a). Stable conformers of PTA (A, B, C, and D) corresponding to the minima on potential energy surface are shown in Fig. 1(b) with their respective ground state energies. It is interesting to note that pair of conformers (A and B; C and D) differ from each other by the rotation of thiadiazole ring by 180° around C5–C6 bond while the pair (A and C; B and D) by rotation of NH_2 group around C2–N12 bond. The rotational barrier of NH_2 group calculated at B3LYP/6-311++G(d,p) level as shown in Fig. 2 is calculated to be 5.680839 kcal/mol. Eigen values obtained from the scan output reveals that, the structure (B) positioning the dihedral N4–C5–C6– C11/N3–C2–N12–H17 at 0°/(150° and −150°), possesses minimum (least) energy at −887.68185262 Hartree. As the energy difference between conformers is very small, we optimized these conformers at a potentially high-level method G2MP2 [36] which uses second order Moller Plesset perturbation theory, to get accurate relative energies. The G2(MP2) energy is sum of E_{base}, ΔE (*MP*2) and ZPE; where of $E_{base} = E$ [*QCISD* (*T*)/ 6-311G(d,p)]; ΔE (*MP*2) = *E* [*MP*2/6-311+G(3df,2p)] − *E* [*MP*2/6-311G(d,p)]; and HCL(High level Correction) = $-0.00481n_\beta$ - $0.00019n_\alpha$ (with number of α electrons $n_\alpha \geq$ number of β electrons n_β) with ZPE = zero point energy. The energy of conformers at G2MP2 is calculated to be −886.240400; −886.240401; −886.240402 and −886.240404 a.u. respectively. This very small difference (almost negligible) in energy indicates the possible co-existence of all four conformers at room temperature. The most stable B conformer at B3LYP level was optimized at M06-2X level also. The ground state energy at M06-2X is calculated to be −887.45497340 Hartree. The optimized bond lengths, bond angles and dihedral angles at B3LYP and M06-2X functionals are compared with the experimental data of similar system [15] due to non-availability of crystal structure and are listed in Table 2. In the six-membered pyridinyl ring all the C–C and C–H bond distances at B3LYP are in the range 1.392–1.402 Å and 1.082–1.086 Å respectively, whereas C8–N9 and C10–N9 bond distances are 1.335 and 1.339 Å, close to the C–N bond length of pyridine 1.338 Å [37]. These values at M06-2X are not much different. A comparison of the optimized parameters at two functionals are presented in Fig. 3 The value of bond angle C10–N9–C8 calculated at B3LYP and M06-2X is nearly same at 116.8° and 117.0° moreover the average C–C–C angle in pyridinyl ring also differ by the same amount. In the hetero thiadiazole moiety, the C–S bond lengths are in between the standard bond lengths for a C–S single bond (1.820 Å) bond and for C=S

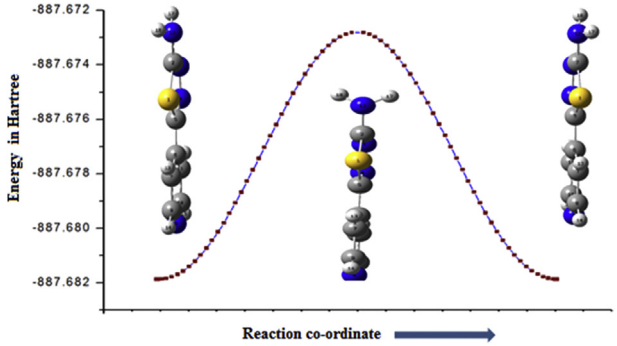

Fig. 2. Rotational barrier of NH_2 group at B3LYP/6-311++G(d,p) level.

Table 2
Computed optimized geometrical parameters of 5-(4-Pyridinyl)-1,3,4-thiadiazol-2-amine at B3LYP/6-311++G(d,p) level along with experimental values.

Bond length (A^0)				Bond angle (°)				Dihedral (°)		
	B3LYP	M06-2X	Exp[a]		B3LYP	M06-2X	Exp[a]		B3LYP	M06-2X
S1–C2	1.756	1.742	1.749	S1–C2–N3	114.1	114.2	113.6	S1–C2–N3–N4	0.1	0.0
C2–N3	1.306	1.299	1.320	C2–N3–N4	112.7	112.5	112.2	C2–N3–N4–C5	−0.5	−0.5
N3–N4	1.358	1.357	1.384	N3–N4–C5	114.8	114.3	113.9	N3–N4–C5–S1	0.7	0.8
N4–C5	1.297	1.290	1.300	N4–C5–S1	112.5	113.0	113.3	N4–C5–S1–C2	−0.5	−0.6
C5–S1	1.777	1.757	1.751	C5–S1–C2	85.9	85.9	87.0	C5–S1–C2–N3	0.2	0.3
C2–N12	1.368	1.369	1.337	S1–C2–N12	122.6	122.3	122.0	S1–C2–N12–H18	170.8	170.8
N12–H18	1.011	1.011		N3–C2–N12	123.2	123.3	124.4	S1–C2–N12–H17	31.0	34.6
N12–H17	1.008	1.008		C2–N12–H17	118.2	117.3	–	N3–C2–N12–H17	−152.9	−149.5
C5–C6	1.465	1.468		C2–N12–H18	114.1	113.0	–	N3–C2–N12–H18	−13.1	−13.2
C6–C7	1.399	1.393		H17–N12–H18	114.9	114.3	–	N4–N3–C2–N12	−176.3	−176.2
C7–C8	1.392	1.391		S1–C5–C6	123.4	123.2	122.5	C5–S1–C2–N12	176.7	176.6
C8–N9	1.335	1.330		N4–C5–C6	124.1	123.8	124.2	S1–C5–C6–C11	−179.6	−179.1
N9–C10	1.339	1.335		C5–C6–C7	122.6	122.3		N4–C5–C6–C7	−179.8	−179.4
C10–C11	1.389	1.387		C5–C6–C11	120.0	119.7		N3–N4–C5–C6	−179.1	−179.0
C11–C6	1.402	1.396		C6–C7–C8	119.0	118.7		C2–S1–C5–C6	179.3	179.1
C7–H13	1.084	1.084		C7–C8–N9	123.8	123.8		C5–C6–C7–C8	−180.0	−180.0
C8–H14	1.086	1.085		C8–N9–C10	116.8	117.0		C5–C6–C11–C10	−180.0	−180.0
C10–H15	1.086	1.085		N9–C10–C11	124.1	124.0		S1–C5–C6–C7	0.5	0.9
C11–H16	1.082	1.082		C10–C11–C6	118.8	118.5		N4–C5–C6–C11	0.2	0.6
				C11–C6–C7	117.4	118.0		C5–C6–C11–H16	0.0	0.0
				C6–C7–H13	121.5	121.6		C5–C6–C7–H13	0.1	0.1
				C8–C7–H13	119.5	119.7		C6–C11–C10–N9	0.0	0.0
				C7–C8–H14	119.9	120.0		C11–C10–N9–C8	0.0	0.0
				N9–C8–H14	116.2	116.2		C10–N9–C8–C7	0.0	0.0
				N9–C10–H15	116.0	116.0		C8–N9–C10–H15	−180.0	−180.0
				C10–C11–H16	121.1	121.4		C10–N9–C8–H14	180.0	180.0
				C11–C10–H15	119.9	119.9		N9–C8–C7–H13	179.9	179.9
				C6–C11–H16	120.1	120.1		N9–C8–C7–C6	0.0	−0.1
								C8–C7–C6–C11	0.1	0.1
								C7–C6–C11–C10	0.0	0.0
								S1–C2–N3–N12	176.4	176.2

[a] Ref [15].

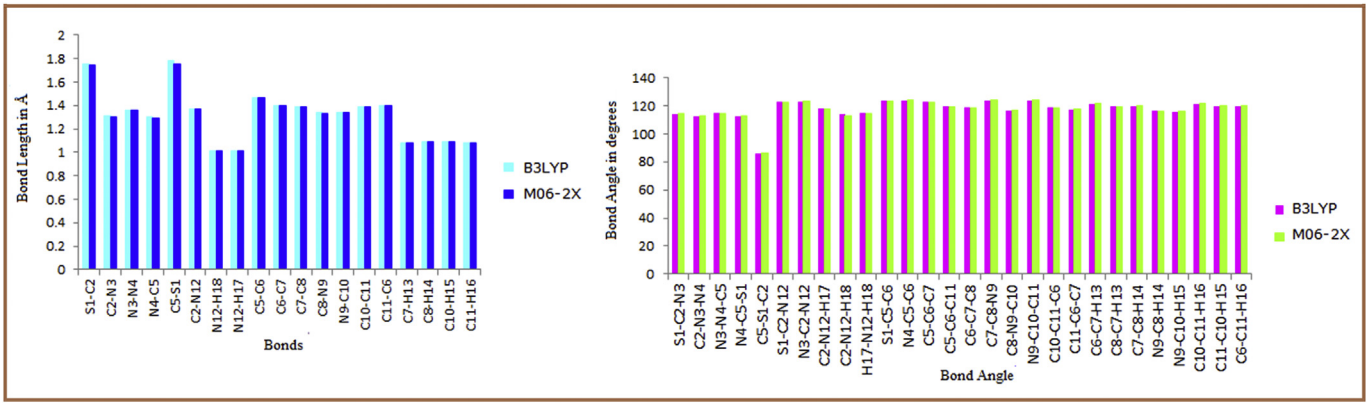

Fig. 3. Comparative graph of optimized parameters at two functionals B3LYP and M06-2X.

double bond (1.61 Å) bond. The C5–S1 (1.777 Å) bond length is the longer than C2–S1(1.756 Å) while C5–N4 (1.297 Å) is the shorter than C2–N3 (1.306 Å). The N12 atom of the amino group is almost 3.6° lower from the plane of the thiadiazole moiety, the dihedral S1–C2–N3–N12 being 176.4°.

3.2. Vibrational analysis

The title compound consists of 18 atoms, which undergo 48 normal modes of vibrations. The molecule possesses C_1 symmetry. The vibrational assignments have been made at B3LYP/6-311++G(d,p) level for which the molecular structure is more stable (minimum energy). A detailed vibrational description is presented by means of normal coordinate analysis, with specific assignment to each wavenumber, attempted through potential energy distribution (PED). For this purpose a set of internal coordinates are defined and given in Table S1. The local symmetry coordinates for PTA were defined as recommended by Fogarasi and Pulay [38] and are presented in Table S2. The method is useful for determining the mixing of other modes, but the maximum contribution is accepted to be the most significant mode. The observed FT-IR, FT-Raman bands with their relative intensities and calculated wave numbers and assignments are given in Table 3. The experimental FT-Raman and FT-IR spectra of PTA along with simulated spectra at B3LYP and M06-2X level have been presented in Fig. 4. It is worth mentioning here that for the title molecule both

Table 3
Comparison of experimental infrared wave numbers (cm^{-1}) with theoretical harmonic frequencies (cm^{-1}), infrared intensities, Raman scattering activities and Raman intensities of molecule 5-(4-Pyridinyl)-1,3,4-thiadiazol-2-amine along with the assignments of vibrational modes basing on PED results.

S. No.	Calculated scaled wavenumbers		Experimental wavenumbers		M06-2X			B3LYP			Assignment of dominant modes in order of decreasing Potential energy distribution (PED > 5%)
	M06-2X	B3LYP	FT-IR	FT-Raman	IR Intensity	Raman Intensity	Raman Activity	IR Intensity	Raman Intensity	Raman Activity	
1	3555	3527			55.8	93.7	61.7	46.7	106.9	69.4	$\nu_{asy}(NH_2)$ (98)
2	3444	3419	3326m	3310w	98.8	467.0	289.5	90.6	583.5	356.7	$\nu_{sy}(NH_2)$ (97)
3	3103	3078	3274m	3061m	2.3	127.9	65.4	2.0	132.8	67.0	$\nu(CH)(R_2)$ (99)
4	3079	3045			3.5	187.8	94.8	7.4	192.4	95.2	$\nu(CH)(R_2)$ (99)
5	3058	3023	3041s	3043m	9.0	253.1	126.2	17.9	316.3	154.5	$\nu(CH)(R_2)$ (99)
6	3056	3019	2937s	2941w	18.3	225.8	112.4	23.7	256.0	124.7	$\nu(CH)(R_2)$ (99)
7	1645	1614	1648vs	1591m	45.4	1420.0	269.9	165.3	36.2	6.7	NH_{2sciss} (80)+ν(CN) (11)
8	1620	1603	1598s		328.2	619.3	115.3	127.8	2310.9	423.7	$\nu(CC)(R_2)$ (53)+$\beta(HCC)(R_2)$ (22)+$\nu(CN)(R_2)$ (8)+$\delta''(R_2)$ (7)
9	1613	1565	1592w	1546w	18.4	76.4	14.1	14.6	229.2	40.7	$\nu(CC)(R_2)$ (42)+$\nu(CN)(R_2)$ (26)+$\beta(HCC)(R_2)$ (11)+$\delta'(R_2)$ (8)
10	1556	1509		1495vs	2.6	2475.8	436.0	23.1	1373.1	231.8	$\nu(CN)(R_1)$ (30)+$\beta(HCC)(R_2)$ (26)+ν(CC) (14)+$\nu(CN)(R_2)$ (10)+$\nu(CC)(R_2)$ (10)
11	1532	1494	1497vs		282.6	2346.3	404.2	374.4	2557.2	425.9	$\nu(CN)(R_1)$ (44)+ν(CN) (22)+$\beta(HCC)(R_2)$ (9)+$\beta(NH_2)$ (6)
12	1509	1475	1450vs	1447vs	8.0	247.0	41.7	34.5	3462.6	566.8	$\nu(CN)(R_1)$ (50)+$\beta(HCC)(R_2)$ (23)+$\delta''(R_1)$ (7)+$\nu(CN)(R_2)$ (6)
13	1429	1415	1411vs	1404m	23.7	170.4	26.7	18.9	390.7	60.5	$\beta(HCC)(R_2)$ (59)+$\nu(CC)(R_2)$ (32)
14	1341	1332	1325m	1353w	49.4	29.5	4.2	6.0	189.1	27.0	$\beta(HCC)(R_2)$ (76)+$\nu(CC)(R_2)$ (11)
15	1333	1310		1317m	32.9	152.5	21.8	56.4	104.2	14.6	β(CNH) (34) + ν(CN) (21)+$\nu(CN)(R_1)$ (16)+$\nu(CS)(R_1)$ (14)+$\beta(N)(R_1)$ (9)
16	1288	1260	1276m	1268m	45.1	386.1	52.8	47.1	312.0	41.5	ν(CC) (27)+ $\nu(CN)(R_1)$ (17)+ $\nu(CC)(R_2)$ (14)+β(HCC) (10)+$\nu(NN)(R_1)$ (9)+$\delta_{trig}(R_2)$ (7)
17	1247	1252	1230w		0.6	216.8	28.4	0.7	266.0	35.1	$\nu(CC)(R_2)$ (48)+$\nu(CN)(R_2)$ (44)
18	1232	1222	1214m	1206s	1.6	201.8	26.1	2.6	371.4	47.4	β(HCC) (64)+$\nu(CN)(R_2)$ (19)+$\nu(CC)(R_2)$ (9)
19	1178	1144	1141m	1133vs	20.5	1963.0	239.2	30.2	2681.4	314.6	$\nu(NN)(R_1)$ (44)+$\nu(CN)(R_1)$ (19)+$\delta'(R_1)$ (8)+ $NH_{2\ rock}$ (7)+ν(CN) (6)
20	1105	1095	1090		0.2	20.8	2.3	0.3	33.9	3.8	β(HCC) (48)+$\nu(CC)(R_2)$ (38)+$\nu(CN)(R_2)$ (6)
21	1085	1071	1059s		2.9	2.5	0.3	1.6	17.6	1.9	β(HCC) (34)+$\nu(CN)(R_2)$ (26)+$\nu(CC)(R_2)$ (21)+$\delta_{trig}(R_2)$ (17)
22	1068	1040		1053w	22.0	96.3	10.4	30.4	187.8	19.5	$NH_{2\ rock}$ (41)+$\nu(NN)(R_1)$ (27)+$\nu(CN)(R_1)$ (15)+$\delta''(R_1)$ (6)
23	1009	992	1006w		16.5	569.4	56.9	7.6	776.5	76.0	$\delta_{trig}(R_2)$ (56)+$\nu(CN)(R_1)$ (24)+$\nu(CC)(R_2)$ (18)
24	1006	987			0.2	1.1	0.1	0.2	0.6	0.1	Υ(HCCC) (91)
25	995	982	992m	988vs	8.9	53.5	5.3	20.0	170.3	16.5	$\nu(CC)(R_2)$ (32)+$\delta'(R_1)$ (30)+$\nu(CS)(R_1)$ (12)+$\delta_{trig}(R_2)$ (10)
26	977	961			0.3	1.3	0.1	0.3	1.3	0.1	Υ(HCCC) (83)+$\tau_{puck}(R_2)$ (15)
27	884	868		860w	3.4	0.9	0.1	3.0	1.4	0.1	Υ(HCCC) (98)
28	828	819	826vs	823w	39.5	9.9	0.8	36.1	15.2	1.2	Υ(HCCC) (75)+ΥCCSN(11)
29	789	774	795w	791m	3.3	174.0	12.8	2.5	287.6	20.6	$\delta''(R_1)$ (34)+$\delta'(R_1)$ (19)+ν(CS) (16)+ν(CN) (8)
30	741	736	742w		0.0	0.5	0.0	0.0	0.4	0.0	$\tau_{puck}(R_2)$ (76)+Υ(HCCC) (12)+ΥCCSN(11)
31	690	679	692s	690m	48.6	177.1	11.0	37.7	160.5	9.7	$\delta''(R_2)$ (54)+$\nu(CS)(R_1)$ (19)+$\nu(CC)(R_2)$ (7)
32	681	666			4.7	51.6	3.1	16.8	168.9	10.0	$\delta'(R_2)$ (71)+$\nu(CS)(R_1)$ (12)
33	668	645	661w	672m	7.7	154.6	9.2	8.2	112.6	6.4	$\nu(CS)(R_1)$ (63)+$\delta''(R_1)$ (12)+$\beta(N)(R_1)$ (9) (Range 705–570)
34	632	614	636w	623w	89.5	41.0	2.3	51.7	14.6	0.8	$\tau''(R_1)$ (43)+$\Upsilon(N)$ (R_1) (37)+$NH_{2\ wag}$ (8)+$\tau'(R_1)$ (5)
35	602	599	608w		8.0	41.9	2.2	8.9	34.6	1.8	$\tau'(R_1)$ (48)+$\tau''(R_1)$ (23)+Υ(CCSN) (17)+Υ(CCCC) (6)
36	593	585	588m	577m	0.3	33.9	1.7	0.2	81.1	4.1	$\delta''(R_1)$ (24)+$\delta'(R_1)$ (19)+$\delta''(R_2)$ (13)+$\tau''(R_1)$ (9)+ν(CS) (9)+$\Upsilon(N)$ (R_2) (6)
37	541	524	516w	505w	116.6	221.4	10.0	64.7	156.9	6.8	$\tau'(R_1)$ (23)+τ'R1(18)+Υ(HCCC) (18)+Υ(CCCC) (13)+$\tau''(R_2)$ (13)
38	496	484	505w		137.9	190.0	7.6	222.8	330.9	12.9	$NH_{2\ wag}$ (45)+$\tau'(R_1)$ (10)+$\tau''(R_2)$ (10)+Υ(CCCC) (8)+$\Upsilon(N)(R_1)$ (6)+ν(CS) (6)
39	424	420	438w	438w	7.7	115.2	3.7	5.9	147.3	4.7	β(NCS) (32)+β(CCS) (20)+β(CCC) (13)+ν(CS) (13)
40	378	377		367w	0.0	4.2	0.1	0.0	3.7	0.1	$\tau'(R_2)$ (66)+ $\tau''(R_2)$ (19)+Υ(HCCC) (14)
41	347	346			11.5	21.7	0.5	17.8	53.5	1.3	$\tau''(R_2)$ (27)+Υ(CCSN) (23)+$\delta'(R_1)$ (13)+Υ(NCSN) (8)+ $NH_{2\ wag}$ (7)+τ(C2–N12) (6)
42	335	331			1.9	235.8	5.5	3.1	353.7	8.0	β(NCS) (38)+β(CCC) (15)+ν(CS) (10)+τ(C2–N12) (6)
43	295	291		305w	1.2	282.1	5.4	39.0	66.2	1.2	$NH_{2\ twist}$ (59)+Υ(NCSN) (12)
44	274	289			41.5	130.6	2.2	1.1	354.3	6.6	ν(CC) (21)+ν(CS) (16)+$\delta''(R_2)$ (13)+$\delta'(R_1)$ (12)+β(CCC) (9)+$\delta'(R_2)$ (8)
45	189	186		203w	9.1	169.7	1.6	8.9	157.0	1.4	$\tau''(R_2)$ (28)+$\tau'(R_1)$ (16)+Υ(HCCC) (15)+$\tau'(R_2)$ (11)+$\tau''(R_1)$ (10)+Υ(CCCC) (8)
46	127	122			3.0	47.3	0.2	3.0	53.9	0.2	β(CSN) (51)+β(CCC) (37)
47	78	78			0.4	5.0	0.0	0.4	11.6	0.0	ΥCCSN(45)+Υ(CCCC) (25)+Υ(HCCC) (9)+$\tau''(R_2)$ (6)+$\tau''(R_1)$ (6)
48	26	30			2.2	1527.3	0.4	2.1	1173.2	0.4	τ (C5–C6) (91)

Abbreviations: R1- Thiadiazole ring; R2- Pyridinyl or Pyridyl ring; ν-stretching, sy-symmetric, asy-antisymmetric; δ-deformation, δ' & δ''-antisymmetric deformation; trig-trigonal; β-in plane bending; Υ -out of plane bending; wag-wagging; rock-rocking; τ-torsion, τ' & τ''-antisymmetric torsion; puck-puckering; sciss-scissoring; twist-twisting; RBM-ring breathing mode.

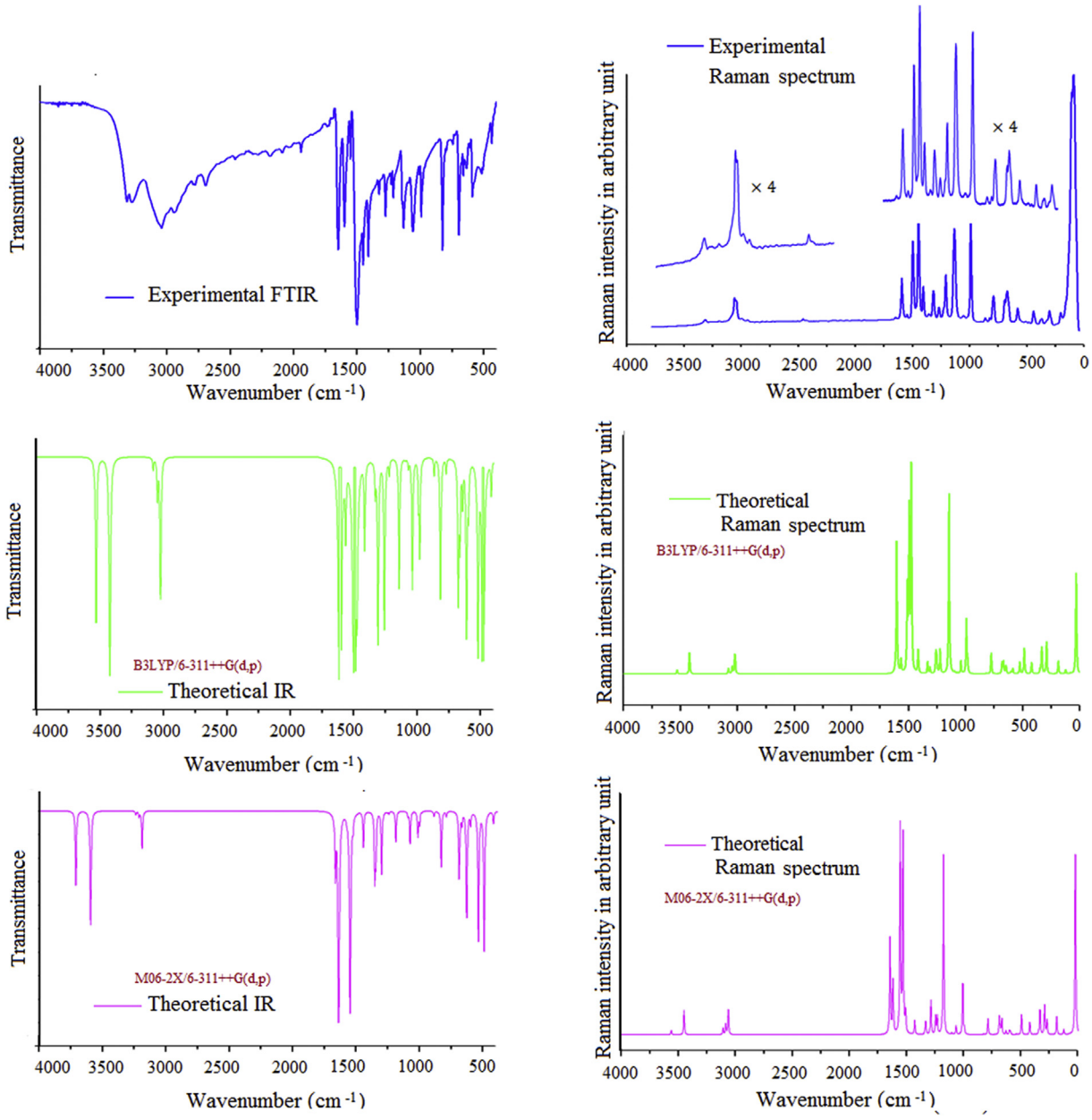

Fig. 4. The experimental FT-Raman and FT-IR spectra of PTA along with simulated Spectra.

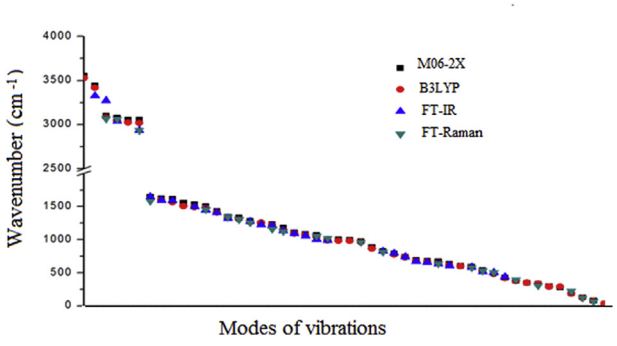

Fig. 5. Correlation graph between calculated (scaled) and the experimental frequencies of PTA.

B3LYP and M06-2X wavenumbers are in good agreement with experimental ones (Fig. 5), M06-2X functional is reproducing better spectral features in terms of line intensity as compared to B3LYP. The title compound consists of a thiadiazole ring substituted by pyridinyl ring and an amino group; hence the vibrational modes are discussed under three heads: (i) NH_2 group vibrations (ii) Pyridinyl or Pyridyl ring vibrations (iii) Thiadiazole ring vibrations.

3.2.1. NH_2 group vibrations

The vibrations exhibited by amino group are - stretching, scissoring and rocking along with inversion and torsion modes. The N–H stretching vibrations in primary amines generally occur in the region 3500–3300 cm^{-1} [39–41]. The medium intensity band at 3326 cm^{-1} in FT-IR and weak band at 3310 cm^{-1} in FT-Raman spectra of PTA, are assigned as N–H stretching mode. The corresponding theoretical scaled wavenumbers for N–H stretching

modes are calculated to be at 3527, 3419 cm^{-1}/3555, 3444 cm^{-1} at B3LYP/M06-2X. The noticeable positive deviation of 93 cm^{-1} in FT-IR at B3LYP and 118 cm^{-1} at M06-2X in computed and observed wavenumbers may be due to involvement of NH_2 group of the molecule in intermolecular hydrogen bonding. The wavenumber corresponding to NH_2 scissoring vibration is usually identified in the region 1590–1670 cm^{-1} [42,43] while NH_2 rocking motion is normally observed in the region 1150–1000 cm^{-1} [44] In the title molecule, the NH_2 scissoring mode is assigned at scaled wavenumber 1614 cm^{-1}. A good agreement with very strong/medium band at 1648/1591 cm^{-1} in FT-IR/FT-Raman spectra has been observed. The calculated PED of PTA suggests N–H rocking mode to be at 1040 cm^{-1} (PED 41%) which is well matched with weak experimental FT-Raman band at 1053 cm^{-1}. The NH_2 wagging vibration analogous to the inversion mode of ammonia is so strongly an-harmonic that it cannot be reproduced by the harmonic treatment [45]. The PED analysis of PTA predicts NH_2 wagging vibrations as mixed modes at scaled wavenumbers 496/484 cm^{-1} at M06-2X/B3LYP.

3.2.2. Pyridinyl ring vibrations

The pyridine ring executes C–C, C–H, C–N stretching, C–H in plane and out of plane bending vibrations, trigonal and asymmetric deformations, puckering along with asymmetric torsional vibrations. There are four hydrogen atoms attached to the pyridine ring carbon atoms in PTA. All four C–H stretching vibrations are pure vibrational modes having 99% PED. The calculated values are in good correlation with experimental FT-IR/FT-Raman spectral peaks at 3274/3061, 3041/3043 and 2937/2941 cm^{-1}. The C–N stretching vibration is spread in the region 1252–1071 cm^{-1} while C–C stretch is calculated in wavenumber range 1603–1095 cm^{-1}. The C–H in plane bending is calculated as mixed modes throughout the region 1415-1071 cm^{-1}. Calculated scaled wavenumbers 987, 961, 868 and 819 cm^{-1} are assigned to C–H out-of plane bending vibrations, well matched with absorbance peaks in FT-IR at 826 cm^{-1} and at 860, 823 cm^{-1} in FT-Raman spectrum. The ring breathing mode covers a broad range 750–1000 cm^{-1} in pyridine and its derivatives [46,47] and is found to be sensitive towards the position and nature of substituents. Fan et al. and A. Singh et al. [48,49]. have shown that ring breathing mode of pyridine provides a sensitive 'indirect' indicator of hydrogen bonding and is blue-shifted upon hydrogen bonding. The ring breathing mode in the present case is assigned at scaled wavenumber 982/995 cm^{-1} (B3LYP/M06-2X) with the help of Gaussview animation and PED.

3.2.3. Thiadiazole ring vibrations

The thiadiazole ring containing 3 hetero atoms (two nitrogens and a sulfur) has vibrations corresponding to N–N, C–N and C–S stretching modes. P. Gautam et al. [50]. observed two bands at 1149 cm^{-1} and 1103 cm^{-1} in the Raman spectrum of N-phenyl-5-phenyl-1,3,4-thiadiazole-2-amine as N–N stretching whereas in the IR spectrum these appeared at 1141 cm^{-1} and 1100 cm^{-1}. The N–N stretching vibration is observed at 1121 cm^{-1} by Bezerra et al. [51] and at 1151 cm^{-1} by Crane et al. [52], In the present case, a very strong band observed at 1133 cm^{-1} in FT-Raman spectrum and a medium intensity band at 1141 cm^{-1} in the FT-IR spectrum are assigned to N–N stretching vibrations of thiadiazol ring. The computed wavenumber for this mode is 1144 cm^{-1}. The C–S stretching vibration is of variable intensity, does not give strong band in infrared and as such assignment is not easy in the infrared. The band may be found over the wide region 1035–245 cm^{-1} [17]. The C–S stretching vibration gives prominent band in Raman spectrum and easy to recognize [53]. Computed values are at 645/668 cm^{-1} in B3LYP/M06-2X are assigned to C–S stretching mode, which are well matched with weak band at 661 cm^{-1} in FT-IR spectrum and good medium intensity band in FT-Raman at 672 cm^{-1}. Difficult task of identifying C–N vibrations due to the mixing of several bands is made somewhat simpler by molecular simulation programs and normal mode analysis. Atalay et al. [15]. have assigned C–N stretching vibrations at 1489 and 1465 cm^{-1} in IR spectrum of 2-Amino-5-phenyl-1,3,4-thiadiazole. The modes calculated at 1494 and 1475 cm^{-1} are the C–N stretching modes (more than 40% P.E.D.) which are in good agreement with experimental values. It is a mixed mode having contribution from C–C stretch and C–H bending vibrations. The in-plane C–S–C and N–C–S vibrations are also well matched with the experimental values.

3.3. Electric moments

To predict the nonlinear optical activity of the title compound, components of various electric moments such as dipole moment (μ), polarizability (α) and first order static hyperpolarizability (β) have been calculated using DFT/B3LYP/6-311++G(d,p) method. Calculation of polarizability and first hyperpolarizability (β) is based on finite-field approach. First hyperpolarizability is a third rank tensor that can be described by a $3 \times 3 \times 3$ matrix. All the 27 components of the matrix can be reduced to 10 components due to the Kleinman symmetry [54]. Components of electric moments are defined as the coefficients in the Taylor series expansion of the energy in the external electric field. When the electric field is weak and homogeneous, this expansion becomes

$$E = E^0 - \sum_i \mu_i F_i - (1/2)\sum_{ij} \alpha_{ij} F_i F_j - (1/6)\sum_{ijk} \beta_{ijk} F_i F_j F_k + \ldots\ldots,$$

where E^0 is the energy of the unperturbed molecules, F_i is the field at the origin, μ_i, α_{ij} and β_{ijk} are components of dipole moment, polarizability, and first order static hyperpolarizability, respectively. Total electric dipole moment (μ), mean polarizability $<\alpha>$, and total first order static hyperpolarizability (β_{total}), have been calculated using the x, y, and z components of these electric moments.

Calculated total electric dipole moment (μ), mean polarizability $<\alpha>$ along with total first order static hyperpolarizability (β_{total}) and their components are presented in Table 4. Dipole moment in a molecule is an important property that is mainly used to study the intermolecular interactions involving non-bonded type dipole–dipole interactions, because higher the dipole moment, stronger will be the intermolecular interactions. In the present case calculated total dipole moment of the PTA molecule is −4.895 Debye at B3LYP. The predicted value of mean polarizability (α_{mean}) and total first order static hyperpolarizability (β_{total}) of PTA are found to be 20.167×10^{-24} esu and 10.667×10^{-30} esu respectively at B3LYP. The mean polarizability and total first static hyperpolarizability calculated at M06-2X is respectively 5.74% and 2.62% lower in comparison to values calculated at B3LYP. Frequency-dependent first hyperpolarizability $\beta(-2\omega;\omega,\omega)$, for the second harmonic generation (SHG) at two wavelengths 1064 nm ($\omega = 0.0428$ a.u.) and 1907 nm ($\omega = 0.0239$ a.u.) are calculated to illustrate the frequency-dependence. Calculation shows that the magnitude of the frequency-dependent first hyperpolarizability increases with the increasing frequency from 12.624×10^{-30} to 18.271×10^{-30} e.s.u. (Table 4). The values of $\beta(-2\omega;\omega,\omega)$ for PTA are larger than the corresponding static β_{tot} values and exhibits large frequency dispersion. These electric moments data predict that PTA compound possesses considerable non-linear optical properties.

Table 4
Dipole Moment, Polarizability and first hyperpolarizability data for 5-(4-Pyridinyl)-1,3,4-thiadiazol-2-amine calculated at B3LYP/6-311++G(d,p).

Polarizability (α)	B3LYP	M06-2X		First static hyperpolarizability and frequency-dependent first Hyperpolarizability(β) (B3LYP)				
				B3LYP	M06-2X		$\omega = 0.0239$ a.u.	$\omega = 0.0428$ a.u.
α_{xx}	209.552	191.993	β_{xxx}	−1294.214	962.721	β_{xxx}	1490.7	2145.8
α_{yy}	129.589	125.458	β_{xxy}	138.953	−100.894	$\beta_{xxy,\ \beta xyx}$	−161.9	−238.8
α_{zz}	69.105	67.370	β_{xyy}	73.417	−63.303	$\beta_{xxz,\ \beta xzx}$	−81.4	−107.9
Mean (a.u.)	136.082	128.274	β_{yyy}	63.203	−46.791	β_{xyy}	29.2	41.2
Mean (esu) $\times 10^{-24}$	20.167	19.010	β_{xxz}	25.436	19.799	$\beta_{xyz,\ \beta xzy}$	−3.1	−3.5
Dipole moment			β_{xyz}	−2.490	−2.175	β_{xzz}	−10.0	−9.6
μ_{xx}	−3.827	−1.359	β_{yyz}	2.955	2.522	β_{yxx}	−157.8	−216.0
μ_{yy}	−2.936	−1.169	β_{xzz}	9.864	−6.987	$\beta_{yxy,\ \beta yyx}$	−78.8	−94.6
μ_{zz}	0.833	0.3687	β_{yzz}	35.611	−33.817	$\beta_{yxz,\ \beta yzx}$	−66.5	−71.1
μ_{Total} (D)	4.895	4.652	β_{zzz}	10.910	9.481	β_{yyy}	−3.1	−3.7
			β_{TOTAL}(a.u.)	1234.681	911.256	$\beta_{yyz,\ \beta yzy}$	3.3	4.1
			β_{TOTAL} (esu) $\times 10^{-30}$	10.667	7.872	β_{yzz}	−38.8	−43.3
						β_{zxx}	29.2	40.4
						$\beta_{zxy,\ \beta zyx}$	−3.1	−3.5
						$\beta_{zxz,\ \beta zzx}$	3.3	3.9
						β_{zyy}	−11.5	−16.4
						$\beta_{zyz,\ \beta zzy}$	−38.9	−43.8
						β_{zzz}	11.7	13.2
						β_{vec} (a.u.)	1461.276	2114.823
						β_{vec} (esu)	12.624 $\times 10^{-30}$	18.271 $\times 10^{-30}$

Table 5
Frontier orbital energies of 5-(4-Pyridinyl)-1,3,4-thiadiazol-2-amine calculated by using TD-DFT/B3LYP/6-311++G(d,p) method.

Energies	Gas	Methanol
E_{TOTAL}(a.u.)	−887.68187	−887.69681
E_{TOTAL}(eV)	−24154.44503	−24154.85162
E_{LUMO} (eV) (MO 47)	−2.18638	−2.24461
E_{HOMO} (eV) (MO 46)	−6.68921	−6.66417
E_{HOMO-1} (eV) (MO 45)	−7.32648	−7.58879
$\Delta E_{(HOMO-LUMO)}$ (eV)	4.50283	4.41956
$\Delta E_{(HOMO-1)-LUMO}$ (eV)	5.14010	5.34418

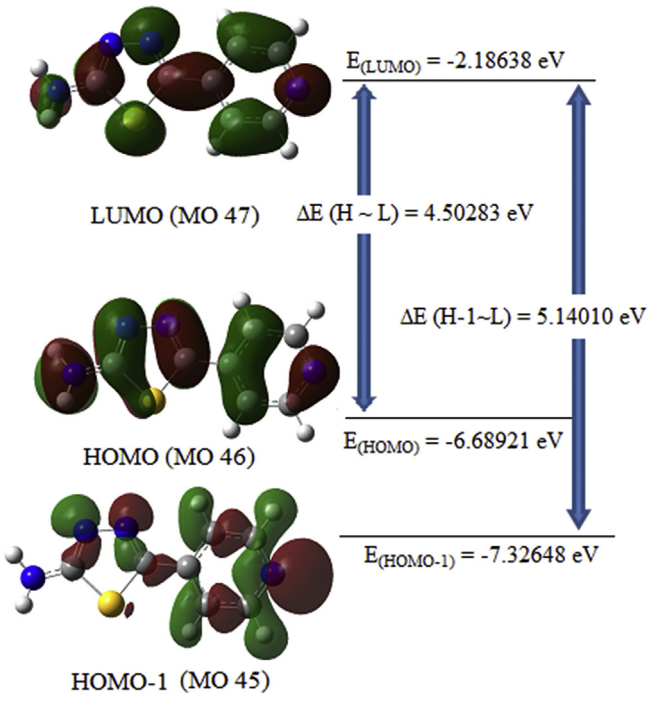

Fig. 6. Patterns of the HOMO, LUMO and other important Molecular Orbitals of PTA obtained with TD-DFT/B3LYP/6-311++G(d,p) method.

3.4. Electronic properties and UV-spectral analysis

The highest occupied molecular orbital (HOMO) and lowest unoccupied molecular orbital (LUMO) are important descriptors in quantum chemistry [55], as these determine the way the molecule interacts with other species. The frontier orbital gap helps characterize the chemical reactivity and kinetic stability of the molecule. The so called "soft molecule" has a small frontier orbital gap, is more polarizable and is generally associated with a high chemical reactivity, low kinetic stability [56]. Fully optimized ground-state structure has been used to determine energies (Table 5) and 3D plots (Fig. 6) of HOMO, LUMO and other MOs involved in the UV transitions of PTA at TD-DFT/B3LYP/6-311++G(d,p) level of theory. It can be seen from figure that both HOMO and LUMO are spread over the entire molecule having contribution from the pyridinyl and thiadiazole rings, but LUMO has more anti-bonding character than HOMO. An ultraviolet spectral analysis of PTA has been made by experimental as well as theoretical calculations (Fig. 7). In order to understand electronic transitions of compound, TD-DFT calculations on electronic absorption spectra in gas phase and methanol solvent were performed. The calculated absorption wavelengths (λ), oscillator strengths (f) and vertical excitation energies (E) for gas phase and solvent (methanol) were carried out and compared with experimental values (Table 6). The calculated absorption maxima have been found to be at 300 and 311 nm wavelength for gas phase and methanol solution respectively. This intense electronic transitions with an oscillator strength f = 0.4827, is in good agreement with the measured experimental data (λ = 316 nm in methanol). This electronic absorption corresponding to the transition from the molecular orbital HOMO (46) to the LUMO (47) excited state, is a $\pi \rightarrow \pi^*$ transition.

Site specific intermolecular hydrogen bonding between hydrogen donor and acceptor molecules plays an important role in determining the structure and reactivity of molecular systems [57,58]. To investigate site specific solute-solvent intermolecular electron transfer interaction we have studied the possible hydrogen bonding between PTA and methanol solvent. There are four possible sites for hydrogen bonding (i) N9––H-O, i.e. hydrogen bonding between N9 of pyridine ring and H–O group of methanol resulting in $[PTA\text{-}MeOH]_a$ (ii) N3––H-O i.e. hydrogen bonding

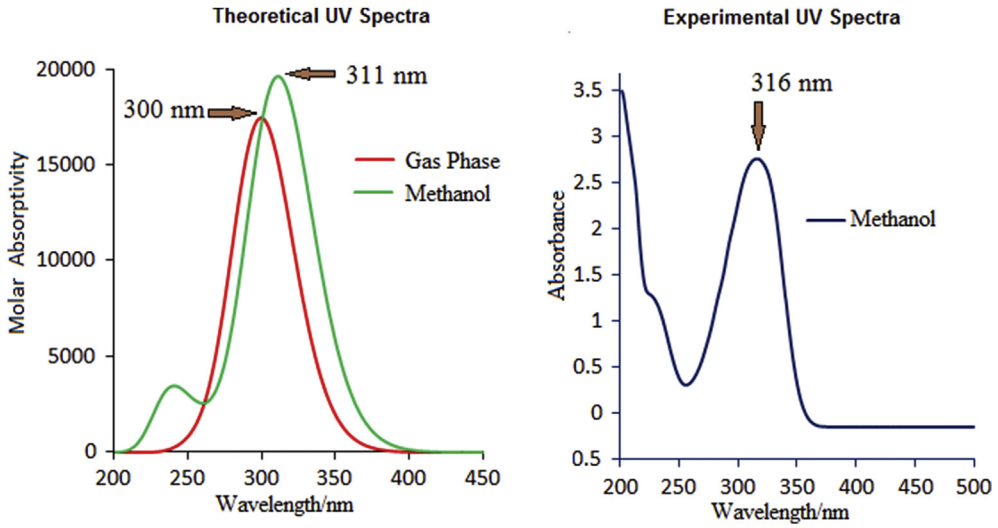

Fig. 7. Experimental and simulated UV absorption spectra of PTA.

Table 6
Experimental and calculated absorption wavelength λ (nm), excitation energies E (eV), absorbance values and oscillator strengths (f) of 5-(4-Pyridinyl)-1,3,4-thiadiazol-2-amine.

Experimental		TD-DFT/B3LYP/6-311++G(d,p)			Major contribution (>10%)
λ(nm)	E(ev)	λ(nm)	E(eV)	f	
Gas					
		301	4.1220	0.1910	H-1→LUMO (52%), HOMO→LUMO (45%)
		300	4.1385	0.2339	H-1→LUMO (45%), HOMO→LUMO (53%)
		280	4.4213	0.0050	H-3→LUMO(96%)
		265	4.6795	0.0193	H-2→ LUMO(75%),HOMO→ L+2(20%)
		260	4.7699	0.0028	HOMO→L+1(88%)
		243	5.1015	0.0000	H-1→L+2(91%)
Methanol					
316	3.9280	311	3.9813	0.4827	HOMO→LUMO(98%)
		288	4.3100	0.0013	H-1→LUMO(97%)
		272	4.5523	0.0040	H-3→LUMO(97%)
		265	4.6709	0.0256	H-2→LUMO(73%)
		246	5.0381	0.0015	HOMO→L+2(95%)
		239	5.1961	0.0789	H-4→LUMO(31%),H-2→LUMO(15%), HOMO→L+1(50%)

Excited states	$[PTA\text{-}MeOH]_a$ E in eV (f) Major contribution	$[PTA\text{-}MeOH]_b$ E in eV (f) Major contribution	$PTA\text{-}(MeOH)_2]_c$ E in eV (f) Major contribution	$[PTA\text{-}(MeOH)_2]_d$ E in eV (f) Major contribution
S_1	3.8259 (0.0018) HOMO→LUMO (70%)	4.0570 (0.4301) HOMO→LUMO (70%)	3.8366 (0.4266) HOMO→LUMO (70%)	4.0228 (0.0098) HOMO-2→ LUMO+1(52%)
S_2	4.0568(0.4455) H-1→LUMO(69%)	4.1597 (0.0040) H-1→LUMO(70%)	4.2078 (0.0003) H-1→LUMO (70%)	4.0750 (0.3997) HOMO→LUMO(69%)
S_3	4.2234(0.0062) H-2→LUMO (64%)	4.5560 (0.0037) H-4→LUMO (49%)	4.4158 (0.0020) H-2→LUMO (66%)	4.1961 (0.0024) HOMO-1→LUMO (53%)
S_4	4.4324(0.0027) HOMO-3→ LUMO(63%)	4.6775(0.0173) H-2→LUMO (59%)	4.4631 (0.0019) HOMO→L+1 (62%)	4.6008 (0.0264) HOMO-3→LUMO+1(64%)
S_5	4.6973(0.0162) HOMO-4→ LUMO(58%)	4.6987(0.0021) HOMO →LUMO+2(66%)	4.5979 (0.0059) HOMO→L+2 (52%)	4.6912 (0.0032) HOMO→ LUMO+1(46%)
S_6	4.7912(0,0023) HOMO → LUMO+2(66%)	5.0298 (0.0002) H-2→LUMO (50%)	4.8029 (0.0001) HOMO→L+4 (52%)	4.7331 (0.0024) HOMO→ LUMO+1(48%)

between N3 of thiadiazole ring and H—O group of methanol forming 6 membered ring N3—C2—N12—H18—H—O labeled as $[PTA\text{-}MeOH]_b$ (iii) hydrogen bonding between amino group and two alcohol molecules constituting $[PTA\text{-}(MeOH)_2]_c$ (iv) two methanol molecules interacting with N3 and N4 of thiadiazole ring resulting in $[PTA\text{-}(MeOH)_2]_d$ To comprehend the nature of electronically excited states for the hydrogen bonded PTA—methanol complexes, TDDFT method has been used to calculate the low lying excited states and their corresponding oscillator strengths, are given in the lower part of Table 6. All the four complexes have been optimized at DFT/B3LYP/6-311++G(d,p). TDDFT calculations yield no significantly energetically lower state for $[PTA\text{-}MeOH]_b$ and $[PTA\text{-}(MeOH)_2]_d$. Although with both $[PTA\text{-}MeOH]_a$ and $[PTA\text{-}(MeOH)_2]_c$, approximately 0.3 eV energetically lower excited state is obtained below the lowest excited state of PTA. This is in line with the S_1 excited state of PTA in methanol solvent. Among these two cases, formation of $[PTA\text{-}MeOH]_a$ is more probable as indicated by pictures of the frontier molecular orbitals of $[PTA\text{-}MeOH]_a$ (Fig. 8). It

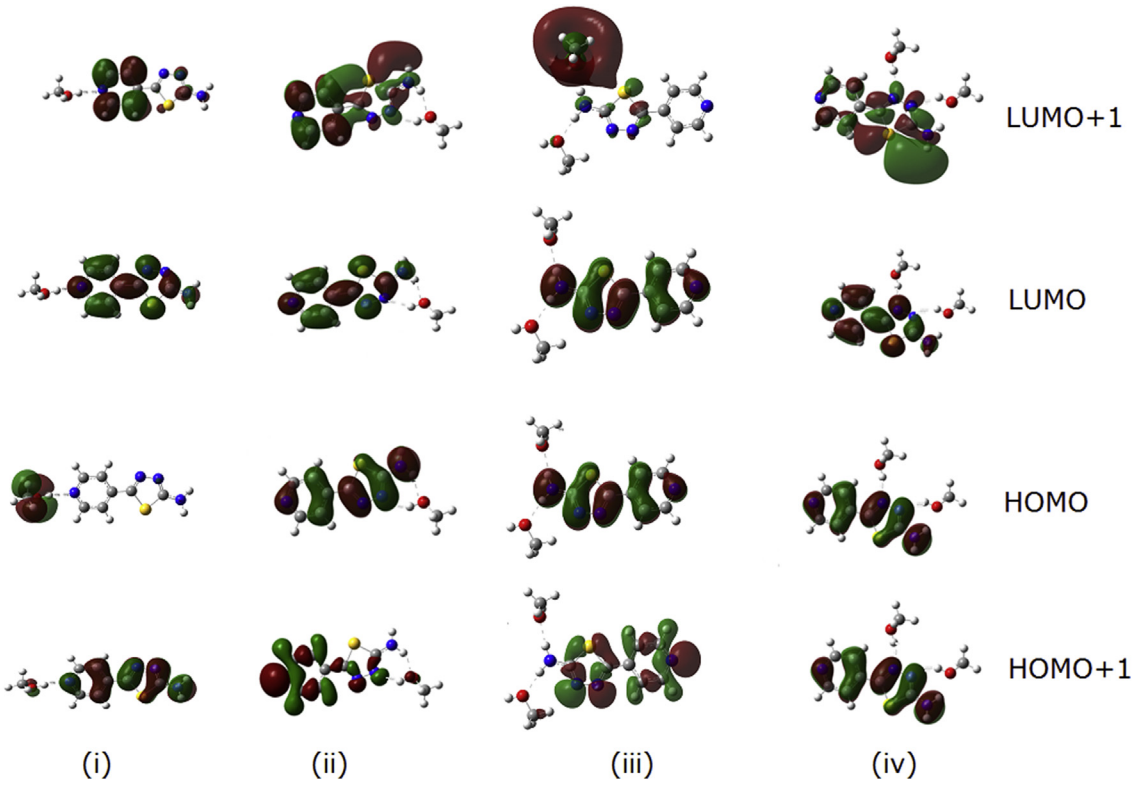

Fig. 8. Frontier molecular orbitals of hydrogen-bonded PTA-MeOH complexes (dashed line denote hydrogen bonds).

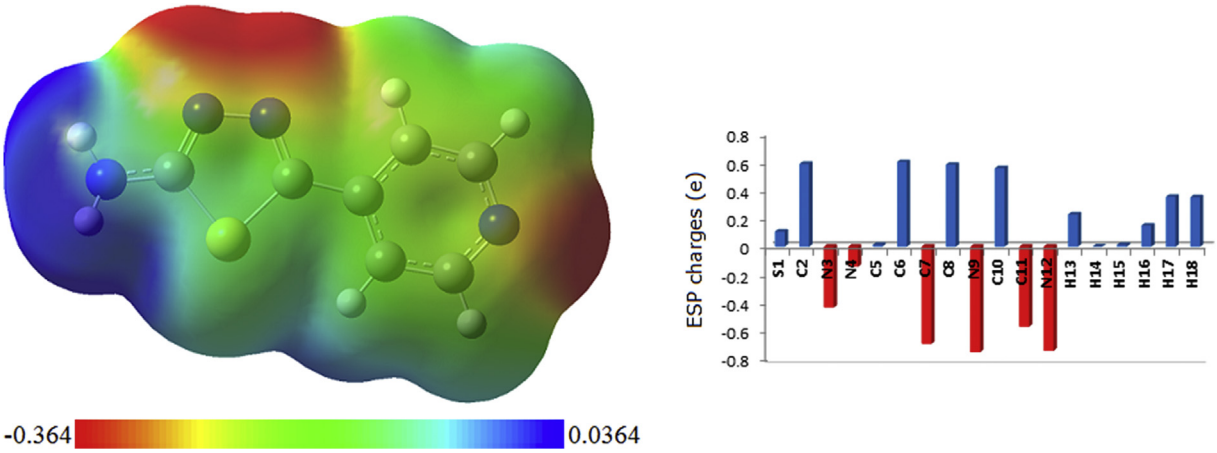

Fig. 9. MESP map and ESP charges of PTA.

can be seen that the electron density of HOMO is localized over the methanol molecule which is bonded by OH—N while densities of other MOs are always localized over PTA. Moreover Table 6 shows the S_1 excited state of $[PTA\text{-}MeOH]_a$ corresponds to the transition from HOMO→LUMO. We can conclude that an energetically lower intermolecular charge transfer (ICT) excited state exists and the electron transfer to this ICT state takes place through H—O——N hydrogen bond.

The MESP may be employed to distinguish regions on the surface which are electron rich (subject to electrophilic attack) from those which are electron poor (subject to nucleophilic attack) and has been found to be a very convenient tool in exploration of correlation between molecular structure and the physiochemical property relationship of molecules including bio molecules and drugs [59–64]. The MESP map of PTA (Fig. 9) clearly suggests that the electron rich (red) region is spread around nitrogen atoms of both pyridinyl and thiadiazole ring, whereas the hydrogen atoms of amino group show the maximum brunt of positive charge (blue). Calculated ESP charges (Fig. 9) show that N9 of pyridinyl moiety has more negative charge as compared to N3 and N4 of thiadiazole ring therefore most probable site for interaction with methanol, supporting our results of solute solvent interaction.

3.5. NMR studies

NMR spectroscopy is widely used for structural and functional group determination of biological macromolecules and is one of the most important aspects of various spectroscopic characterization

Table 7
H^1-NMR Chemical shift (ppm) for title molecule with respect to TMS.

Atom No.	Experimental		DFT/B3-LYP/6-3111++G(d,p)				
	(Chloroform-D)	Gas phase	Chloroform				
			Conf. B	Conf. A	Conf. C	Conf. D	Average
H13	7.063	7.084	7.462	8.404	8.401	7.085	7.838
H14	7.425	8.759	8.805	8.844	8.840	8.760	8.812
H15	7.439	8.848	8.831	8.791	8.788	8.848	8.815
H16	7.312	8.380	8.391	7.337	7.329	8.381	7.860
H17	3.248	3.975	4.746	4.462	4.993	4.719	4.730
H18	3.892	4.707	5.061	4.947	4.514	3.978	4.625

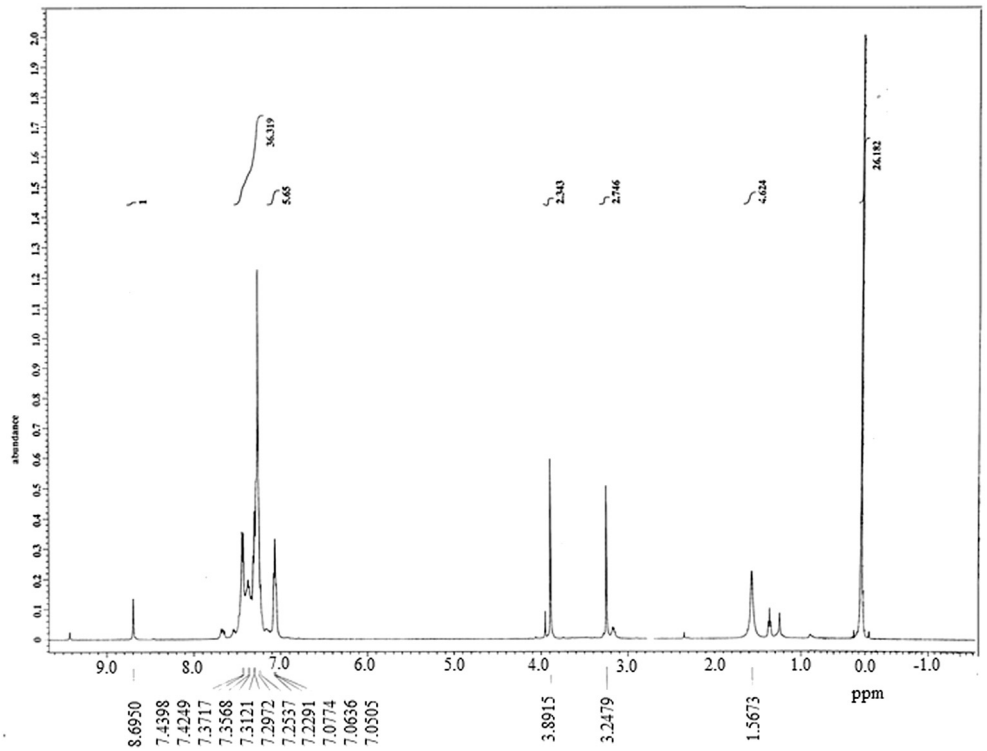

Fig. 10. ^{1}H NMR spectrum of PTA.

techniques. ^{1}H chemical shift of the title molecule have been simulated with the optimized molecular structure at DFT-B3LYP/6-311++G(d,p) level using the Gauge-Including Atomic Orbital (GIAO) method. The calculated ^{1}H chemical shifts for the proton atoms of title molecule in gas phase as well as in $CDCl_3$ solvent, taking tetramethylsilane (TMS) as a reference, is given in Table 7 along with the experimentally observed values. The recorded ^{1}H -NMR spectrum of PTA compound in $CDCl_3$ solution is shown in Fig. 10.

There are six hydrogen atoms (4 attached to pyridinyl ring and 2 to amino group) in the title compound. Chemical shifts in region 6.0–8.0 ppm in ^{1}H-NMR spectrum usually appeared due to nuclear magnetic resonances of aromatic protons and indicate the presence of aromatic hydrogen in the compound. The electronegative nitrogen atom present in the pyridinyl ring, decrease the shielding and increases the chemical shift from the normal aromatic ring range. Chemical shift corresponding to pyridinyl hydrogen atoms are experimentally observed in the range 7.063–7.439 ppm while the calculated values are in the range 7.462–8.831. Simulated chemical shift for H17 and H18 atoms of amino group in title molecule are found to be 4.746 and 5.061 ppm respectively while corresponding shift line in experimental spectrum is observed at 3.248 and 3.892 ppm respectively. The deviation between predicted and observed shift values may be due to the involvement of the amino group atoms in intermolecular hydrogen bonding which causes shifting of corresponding resonances towards lower nuclear field or may be due to the presence of all conformers at room temperature. To substantiate this, we have carried out DFT calculations for PTA-($2H_2O$) where amino group of PTA is hydrogen bonded to two water molecules. After optimization of PTA-($2H_2O$), NMR shifts were calculated. The chemical shifts of PTA-($2H_2O$) for H17 and H18 were found to be 8.201 and 7.597 ppm, far away from the experimental values, ruling out the possibility of participation of the amino group atoms in intermolecular hydrogen bonding. The NMR chemical shifts of remaining three conformers (A, C and D) were then calculated and found to be different for different conformations. The average NMR chemical shifts due to the four conformers are in better agreement with the experimental values. We may conclude the presence of all four conformers at room temperature and the observed chemical shift may be the weighted average of the shifts of the individual conformations.

Table 8
Second order perturbation theory analysis of Fock matrix in NBO Basis for 5-(4-Pyridinyl)-1,3,4-thiadiazol-2-amine.

Donor(i)	Type	ED(i) (e)	Acceptor(j)	Type	ED(j) (e)[a]	E(2)[b] Kcal/mol	E(j) - E(i)[c] (a.u.)	F(i,j)[d] (a.u.)
S1–C5	σ	1.97640	C2–N12	σ*	0.02460	5.62	1.09	0.070
C2–N3	π	1.87246	N4–C5	π*	0.32849	14.41	0.33	0.065
N4–C5	π	1.89422	C2–N3	π*	0.39136	9.68	0.32	0.054
N4–C5	π	1.89422	C6–C7	π*	0.37399	10.08	0.36	0.058
C6–C7	π	1.63518	N4–C5	π*	0.32849	18.44	0.26	0.062
C6–C7	π	1.63518	C8–N9	π*	0.37381	27.44	0.27	0.077
C6–C7	π	1.63518	C10–C11	π*	0.27331	15.94	0.29	0.062
C8–N9	π	1.71245	C6–C7	π*	0.37399	13.34	0.32	0.059
C8– N9	π	1.71245	C10–C11	π*	0.27331	25.40	0.32	0.081
C10–C11	π	1.63567	C6–C7	π*	0.37399	23.48	0.28	0.072
C10–C11	π	1.63567	C8–N9	π*	0.37381	17.47	0.27	0.061
N12–H18	σ	1.98072	S1–C2	σ*	0.08213	6.51	0.84	0.067
S1	LP 2	1.66822	C2–N3	π*	0.39136	27.98	0.25	0.076
S1	LP 2	1.66822	N4–C5	π*	0.32849	23.71	0.26	0.070
N3	LP 1	1.89917	C2	RY*(1)	0.00912	5.31	1.22	0.074
N3	LP 1	1.89917	S1–C2	σ*	0.08213	15.19	0.56	0.083
N3	LP 1	1.89917	N4–C5	σ*	0.02713	5.50	0.95	0.066
N4	LP 1	1.89285	S1–C5	σ*	0.08473	16.44	0.55	0.085
N4	LP 1	1.89285	C2–N3	σ*	0.03166	5.43	0.93	0.065
N9	LP 1	1.91827	C7 –C8	σ*	0.02524	9.22	0.90	0.083
N9	LP 1	1.91827	C10–C11	σ*	0.02412	8.96	0.91	0.082
N12	LP 1	1.80559	C2–N3	π*	0.39136	37.73	0.30	0.099

[a] ED: Electron Density.
[b] E(2) means energy of hyperconjugative interactions.
[c] Energy difference between donor and acceptor i and j NBO orbitals.
[d] F(i,j) is the Fock matrix element between i and j NBO orbitals.

3.6. NBO analysis

The calculation pertaining to delocalization of the electron density between occupied Lewis type (bond (or) lone pair) NBO orbitals and formally unoccupied (anti-bond (or) Rydberg) non-Lewis NBO orbitals corresponding to a stabilizing donor–acceptor interactions, have been performed at B3LYP/6-311++G(d,p) basis set. The energy of these interactions can be estimated by the second order perturbation theory [65]. Table 8 lists the calculated second-order interaction energies (E(2)) between the donor–acceptor orbitals in PTA. The larger E(2) (energy of hyper-conjugative interaction) value, the more intensive is the interaction between electron donors and acceptors i.e., the more donation tendency from electron donors to electron acceptors and the greater the extent of conjugation of the whole system. The interaction formed by the orbital overlap between bonding π (C–C) of the pyridinyl ring and antibonding (C–C), (C–N) orbitals of the same, results in intra-molecular charge transfer (ICT) leading to the stabilization of the system. Table 8 clearly shows that the strong hyper conjugative interaction of π electrons of (C6–C7) with π*(C10–C11), π*(C8–N9), and of π (C10–C11) with π*(C6–C7), π*(C8–N9) contribute to stabilization of pyridinyl ring. On the other hand, very strong interactions have been observed between the p type orbitals of S1 containing the lone electron pair with the neighboring π*(C2–N3) and π*(N4–C5) antibonding orbitals of thiadiazole ring. The interaction of p electrons of C2, N3, N4 and C5 with the second lone pair of S1 plays a decisive role in stabilization of the system as evident from the deviation in ideal Lewis structure of occupancy 2.00 to 1.67. An important contribution for the molecular stabilization is further given by LP1 of N3 and N4 conjugated with σ*(S1–C2), σ*(S1–C5) having energy contribution of 15.19 and 16.44 kcal/mol respectively. LP1(N12) of NH_2 group conjugated with π*(C2–N3) brings about the stabilization of the system by 37.73 kcal/mol.

3.7. Thermo-dynamical analysis

On the basis of vibrational analysis, the statistical thermodynamic functions: heat capacity ($C^0_{p,m}$) entropy (S^0_m) and enthalpy changes (ΔH^0_m) at different temperatures (100–700 K) along with Zero point vibrational energy (80.56658 kcal/mol) and rotational constants at standard temperature (298.15 K) for the title compound were obtained using DFT-B3LYP/6-311++G(d.p) method and listed in Table S3. The correlation between these thermodynamic properties and temperatures is shown in Fig. 11. As observed from Table S3, the values of heat capacity, entropy and enthalpy increases with the increase of temperature from 100 to 700 K, which is attributed to the enhancement of molecular vibrational intensities with the temperature. The correlation equations between heat capacity, entropy, enthalpy changes and temperatures were fitted by quadratic formulas and the corresponding fitting factors (R^2) for these thermodynamic properties are 0.999, 1 and 0.999, respectively. The corresponding fitting equations are as follows:

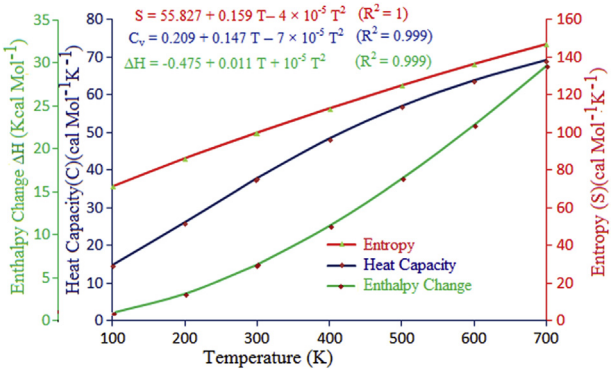

Fig. 11. Correlation graphs of calculated heat capacity, entropy and change in enthalpy for PTA.

$$C^0_{p,m} = 0.209 + 0.147\,T - 7 \times 10^{-5}T^2 \quad \left(R^2 = 0.999\right)$$

$$S_m^0 = 55.827 + 0.159\,T - 4 \times 10^{-5}T^2 \quad \left(R^2 = 1\right)$$

$$\Delta H_m^0 = -0.475 + 0.011\,T + 10^{-5}T^2 \quad \left(R^2 = 0.999\right)$$

All these thermodynamic data may deliver useful information for the further study on the title compound. They are useful in thermo-chemical field as they can be used to compute the other thermodynamic energies and estimate directions of chemical reactions according to relationships of thermodynamic functions and using second law of thermodynamics. It is worth to mention that all thermodynamic calculations were done in gas phase and they could not be used in solution.

4. Conclusions

In the present study, we have carried out the spectroscopic analysis of 2-Amino-5-(4-Pyridinyl)-1,3,4-thiadiazole for the first time using experimental (FT-IR, FT-Raman and UV–Vis) and theoretical (DFT) methods. The optimized geometric parameters and vibrational harmonic wavenumbers, of the compound have been calculated using DFT/B3LYP and M06-2X methods with 6-311++G(d,p) basis set. In general, a good agreement between experimental and the calculated normal modes of vibrations has been observed. Electric moments calculated at B3LYP are 2–5% higher than corresponding values calculated at M06-2X. The increase in frequency-dependent first hyperpolarizability $\beta(-2\omega;\omega,\omega)$ from 12.624 × 10^{-30} to 18.271 × 10^{-30} esu with increase in frequency from 0.0239 a.u. to 0.0428 a.u. suggests NLO character of the title molecule. Investigation of possible complexes of PTA with methanol suggests that site specific hydrogen bonding exist between methanol and PTA which give rise to energetically lower ICT excited state. NMR chemical shifts analysis confirms the presence of all four conformers at room temperature.

Acknowledgments

The authors would like to extend their appreciation to the Deanship of Scientific Research at King Saud University for funding this study through the research group project No. PRG-1436-23. The authors are thankful to IIT Kanpur, India for giving permission for spectral measurements. Prof. T. Sundius is also gratefully acknowledged for his MOLVIB program.

Appendix A. Supplementary data

Supplementary data related to this article can be found at http://dx.doi.org/10.1016/j.molstruc.2015.11.077.

References

[1] N. Demirbas, S.A. Karaoglu, A. Demirbas, K. Sancak, Eur. J. Med. Chem. 39 (2004) 793–804.
[2] H.N. Dogan, A. Duran, S. Rollas, G. Sener, M.K. Uysal, D. Gülen, Bioorg. Med. Chem. 10 (2002) 2893–2898.
[3] E. Palaska, G. Sahin, P. Kelicen, N.T. Durlu, G. Altinok, II Farm. 57 (2002) 101–107.
[4] A. Foroumadi, Z. Kiani, F. Soltani, Il Farm. 58 (2003) 1073–1076.
[5] L. Mishra, V.K. Singh, N.K. Dubey, A.K. Mishra, Biosci. Biotechnol. Biochem. 57 (1993) 989–991.
[6] F. Russo, A. Santagati, M. Santagati, J. Heterocycl. Chem. 22 (1985) 297–299.
[7] S. Masahito, M. Kazuyuki, Agric. Biol. Chem. 41 (1977) 2047–2053.
[8] T. Ramalingam, M. Sre Rama Murty, P.B. Suttur, Heterocycles 29 (1989) 925–932.
[9] N.S. El-Gohary, M.I. Shaaban, Eur. J. Med. Chem. 63 (2013) 185–195.
[10] H.M. Patel, B. Sing, V. Bhardwaj, M. Palkar, M.S. Shaikh, R. Rane, W.S. Alwan, A.K. Gadad, M.N. Noolvi, R. Karpoormath, Eur. J. Med. Chem. 93 (2015) 599–613.
[11] L.M. Weinstock, I. Shinkai, in: K.T. Potls (Ed.), Comprehensive Heterocyclic Chemistry, vol. 6, Pergamon, Oxford, UK, 1984.
[12] K. Mullen, G. Wegner, Electronic Materials: the Oligomer Approach, Wiley-VCH, Weinheim, FRG, 1998.
[13] G.E. Cami, E.E. Chufan, J.C. Pedregosa, E.L. Veretti, J. Mol. Struc. 570 (2001) 119–127.
[14] H. Feki, N. Fourati, Y. Abid, C. Minot, J. Mol. Struc. Theochem. 852 (2008) 87–92.
[15] Y. Atalay, F. Yakuphanoglu, M. Sekerci, D. Avcı, A. Basoglu, Spectrochim. Acta A 64 (2006) 68–72.
[16] C. Meganathan, S. Sebastian, I. Sivanesan, K.W. Lee, B.R. Jeong, H. Oturak, S. Sudha, N. Sundaraganesan, Spectrochim. Acta A Mol. Biomol. Spectrosc. 95 (2012) 331–340.
[17] R. John Xavier, P. Dinesh, Spectrochim. Acta A Mol. Biomol. Spectrosc. 113 (2013) 171–181.
[18] S. Chandra, S. Gautam, H.K. Rajor, R. Bhatia, Spectrochim. Acta A 137 (2015) 749–760.
[19] A.A. El-Azhary, Spectrochim. Acta A 51 (1995) 995–1003.
[20] W. Kohn, L.J. Sham, Phys. Rev. A 140 (1965) 1133–1138.
[21] A.D. Becke, J. Chem. Phys. 98 (1993) 5648–5652.
[22] C. Lee, W. Yang, R.G. Parr, Phys. Rev. B 37 (1988) 785–789.
[23] B. Miehlich, A. Savin, H. Stoll, H. Preuss, Chem. Phys. Lett. 157 (1989) 200–206.
[24] Y. Zhao, D.G. Truhlar, Theor. Chem. Acc. 120 (2008) 215–241.
[25] M.J. Frisch, G.W. Trucks, H.B. Schlegel, G.E. Scuseria, M.A. Robb, J.R. Cheeseman, G. Scalmani, V. Barone, B. Mennucci, G.A. Petersson, H. Nakatsuji, M. Caricato, X. Li, H.P. Hratchian, A.F. Izmaylov, J. Bloino, G. Zheng, J.L. Sonnenberg, M. Hada, M. Ehara, K. Toyota, R. Fukuda, J. Hasegawa, M. Ishida, T. Nakajima, Y. Honda, O. Kitao, H. Nakai, T. Vreven, J.A. Montgomery Jr., J.E. Peralta, F. Ogliaro, M. Bearpark, J.J. Heyd, E. Brothers, K.N. Kudin, V.N. Staroverov, R. Kobayashi, J. Normand, K. Raghavachari, A. Rendell, J.C. Burant, S.S. Iyengar, J. Tomasi, M. Cossi, N. Rega, J.M. Millam, M. Klene, J.E. Knox, J.B. Cross, V. Bakken, C. Adamo, J. Jaramillo, R. Gomperts, R.E. Stratmann, O. Yazyev, A.J. Austin, R. Cammi, C. Pomelli, J.W. Ochterski, R.L. Martin, K. Morokuma, V.G. Zakrzewski, G.A. Voth, P. Salvador, J.J. Dannenberg, S. Dapprich, A.D. Daniels, O. Farkas, J.B. Foresman, J.V. Ortiz, J. Cioslowski, D.J. Fox, Gaussian Inc., Wallingford, CT, 2009.
[26] E. Frisch, H.P. Hratchian, R.D. Dennington II, T.A. Keith, J. Millam, A.B. Nielsen, A.J. Holder, J. Hiscocks, GaussView Version 5.0.8, Gaussian, Inc, 2009.
[27] M. Karabacak, M. Kurt, M. Cinar, A. Coruh, Mol. Phys. 107 (2009) 253–264.
[28] N. Sundaraganesan, S. Ilakiamani, H. Saleem, P.M. Wojciechowski, D. Michalska, Spectrochim. Acta A 61 (2005) 2995–3001.
[29] J.B. Foresman, A. Frisch, Exploring Chemistry with Electronic Structure Methods, second ed., Gaussian Inc., Pittsburgh, PA, 1996.
[30] T. Sundius, J. Mol. Spectrosc. 82 (1980) 138–151.
[31] T. Sundius, J. Mol. Struct. 218 (1990) 321–336.
[32] T. Sundius, Vib. Spectrosc. 29 (2002) 89–95.
[33] G. Keresztury, S. Holly, J. Varga, G. Besenyei, A.Y. Wang, J.R. Durig, Spectrochem. Acta 49 (1993) 2007–2017.
[34] G. Keresztury, Raman spectroscopy: theory, in: J.M. Chalmers, P.R. Griffith (Eds.), Handbook of Vibrational Spectroscopy, John Wiley & Sons, New York, 2002.
[35] E.D. Glendening, C.R. Landis, F. Weinhold, WIREs Comput. Mol. Sci. 2 (2011) 1–42.
[36] L.A. Curtiss, K. Raghavachari, J.A. Pople, J. Chem. Phys. 98 (1993) 1293–1298.
[37] K.K. Innes, I.G. Ross, W.R. Moomaw, J. Mol. Spectrosc. 132 (1988) 492–544.
[38] P. Pulay, G. Fogarasi, F. Pang, J.E. Boggs, J. Am. Chem. Soc. 101 (1979) 2550–2560.
[39] A. Altun, K. Golcuk, M. Kumru, J. Mol. Struct. (Theochem) 637 (2003) 155–169.
[40] Y. Wang, S. Saebo, C.V. Pittman, J. Mol. Struct. (Theochem) 281 (1993) 91–96.
[41] N. Puviarasan, V. Arjunan, S. Mohan, Turk. J. Chem. 26 (2002) 323–334.
[42] S.K. Pathak, R. Srivastava, A.K. Sachan, O. Prasad, L. Sinha, A.M. Asiri, M. Karabacak, Spectrochim. A 135 (2015) 283–295.
[43] S.K. Pathak, R. Srivastava, A.K. Sachan, O. Prasad, L. Sinha, Spectrochim. Acta A 143 (2015) 147–157.
[44] G. Varsanyi, Vibrational Spectra of Benzene Derivatives, Academic Press, New York, 1969.
[45] P.M. Wojciechawski, D. Michalska, Spectrochim. Acta A 68 (2007) 948–955.
[46] P.L. Anto, R.J. Anto, H.T. Varghese, C. Yohannan Panicker, D. Philip, Gustavo F.S. Andrade, A.G. Brolo, J. Raman Spectrosc. 42 (2011) 1812–1819.
[47] V.K. Rastogi, M.A. Palafox, Kamil Lang, S.K. Singhal, R.K. Soni, Rekha sharma, Ind. J. Pure App. Phys. 44 (2006) 653–660.
[48] H. Fan, C. Diane Moliva A., J.K. Eliason, J.L. Olson, Daniel D. Green, M.W. Gealy, Darin J. Ulness, Chem. Phys. Lett. 479 (2009) 43–46.
[49] A. Singh, D. Gangopadhyay, Jürgen Popp, Ranjan K. Singh, Spectrochim. A 99 (2012) 136–143.
[50] P. Gautam, Om Prakash, R.K. Dani, N.K. Singh, Ranjan K. Singh, Spectrochim. A 132 (2014) 278–287.
[51] A.C.S. Bezerra, E.L. De Sa, F.C. Nart, J. Phys. Chem. 101 (1997) 6443–6449.
[52] L.G. Crane, D. Wang, L.M. Sears, B. Heynz, K. Carron, Anal. Chem. 67A (1995) 360–364.
[53] N.P.C. Roeges, A Guide to the Complete Interpretation of Infrared Spectra of Organic Structures, Wiley, New York, 1994.
[54] D.A. Kleinman, Phys. Rev. 126 (1962) 1977–1979.
[55] J.M. Seminario, Recent Developments and Applications of Modern Density Functional Theory, Elsevier, Amsterdam, 1996.

[56] I. Fleming, Frontier Orbitals and Organic Chemical Reactions, John Wiley and Sons, NewYork, 1976.
[57] G.J. Zhao, K.L. Han, Acc. Chem. Res. 45 (2012) 404–413.
[58] G.J. Zhao, J.Y. Liu, L.C. Zhou, K.L. Han, J. Phys. Chem. B 111 (2007) 8940–8945.
[59] I. Alkorta, J.J. Perez, Int. J. Quantum. Chem. 57 (1996) 123–135.
[60] E. Scrocco, J. Tomasi, in: P. Lowdin (Ed.), Advances in Quantum Chemistry, Academic Press, New York, 1978.
[61] F.J. Luque, M. Orozco, P.K. Bhadane, S.R. Gadre, J. Phys. Chem. 97 (1993) 9380–9384.
[62] J.S. Murray, K. Sen, Molecular Electrostatic Potentials, Concepts and Applications, Elsevier, Amsterdam, 1996.
[63] R.K. Pathak, S.R. Gadre, J. Chem. Phys. 93 (1990) 1770–1774.
[64] S.R. Gadre, I.H. Shrivastava, J. Chem. Phys. 94 (1991) 4384–4390.
[65] I. Hubert Joe, I. Kostova, C. Ravikumar, M. Amalanathan, S.C. Pinzaru, J. Raman Spectrosc. 40 (2009) 1033–1038.